*applied mechanics*

MDPI

*Article*

# Behavior of Micropile (Type D) Subjected to Vertical Load: Parametric Numerical Studies

**Mo'men Ayasrah**

Department of Civil Engineering, Faculty of Engineering, Al Al-Bayt University, Mafraq 25113, Jordan; ayasrahmomen@aabu.edu.jo

**Abstract:** Micropiles, small-diameter-drilled and grouted piles, are often used to provide foundation support in challenging ground conditions. This research seeks to understand the behavior of Type D micropiles (pressure-grouted) within layered soil profiles. Layered soils frequently create complexity because of differences in stiffness, strength, and permeability, which impact load transfer and the interaction between the micropiles and the surrounding soil. Type D micropiles use pressure injection, which results in enhanced skin friction, better grout–soil contact, and a greater capacity to carry loads. A set of numerical simulations was conducted to analyze the behavior of the micropile Type D under axial loading, which was evaluated by considering factors such as micropile diameter, spacing, and inclination. The results indicated that increasing the diameter of a micropile significantly improves its performance by enhancing load transfer and structural stiffness, as well as reducing soil deformation and settlement. In addition, for vertical micropiles and those with inclination angles of 10° and 20°, stiffness increased with diameter, while axial displacement remained constant at a 45° inclination. Furthermore, larger diameters reduced lateral displacements up to 20° inclination angles by increasing stiffness, but lateral deflection increased at 45° due to greater lateral load components. The bending moment increased with inclination angle, driven by higher horizontal loads and increased eccentricity, while spacing had little effect for angles greater than 20° due to effective load redistribution.

**Keywords:** micropiles; pressure-grouted; numerical simulations; axial displacement; lateral deflection; bending moment



Received: 7 December 2024
Revised: 31 December 2024
Accepted: 8 January 2025
Published: 14 January 2025

**Citation:** Ayasrah, M. Behavior of Micropile (Type D) Subjected to Vertical Load: Parametric Numerical Studies. *Appl. Mech.* **2025**, *6*, 4. https://doi.org/10.3390/applmech6010004



## 1. Introduction

Micropiles are small-diameter pile foundations that are widely used to underpin infrastructure and buildings as well as reinforce preexisting foundations. They are a useful method for reducing settlements, enhancing seismic performance, and raising bearing capacity [1–4]. Recent advancements in research have significantly enhanced the understanding of the complex behavior of pile foundations under diverse operational conditions. These include dynamic loads, seismic responses, and overall structural performance. Such insights have been pivotal in refining methods to evaluate pile behavior, particularly in practical engineering applications [5–7].

Micropile construction involves the installation of reinforcement in boreholes ranging in diameter from 100 mm to 300 mm, followed by the injection of grout into the hole as a final step. Reinforcement, such as steel rebar and hollow bars with high strength, transmits the upper load to the grout body, while the bond strength between the grout body and the ground supports the load. When determining the design capacity of a micropile, one typically ignores the end-bearing capacity due to the pile's small diameter, and instead

considers the skin friction of the pile [8]. The Federal Highway Administration's (FHWA) recommendation is that for micropile design and construction, the primary consideration for determining the design capacity when taking the grouting method into account is the range of bond strength (αbond) values at the pile-to-ground interface (FHWA 2005) [2].

Furthermore, Juran et al. (1999) [9] demonstrated the division of micropiles into two systems: the construction method and the behavior philosophy. According to their design approach, micropiles are divided into two cases by the philosophy of behavior: Case I is directly loaded piles, which may be found alone or in groups, and Case II is the root construction of micropiles, which can be found in networks and three-dimensional reticulated piles. In addition, micropiles are categorized according to the grouting technique used in their formation. This technique impacts the grout's ability to adhere to the ground. The drilling and building methods influence the type of micropile and the load transmission mechanism [10].

The behavior of micropiles has been studied and exploited to provide insights into the micropile performance through field testing and monitoring, large-scale laboratory testing, analytical techniques, and finite element analysis. Several studies have been conducted to investigate the load-carrying behavior and micropile effect [11–15]. These investigations consider many influencing factors, including micropile (MP) inclination, slenderness ratio, MP configuration, and load direction related to the lateral, uplift, and axial load capacities. Design approaches for the engineering application were suggested, and the improved loading-carrying performance of single and group MPs with MP configuration was also examined under varied loading conditions [16].

Abd Elaziz and EI Naggar (2014) [12] suggested interaction factor curves based on a number of criteria, including the properties of the soil and piles, the distance between the micropiles, and the ratio of the micropiles' slenderness. Tsukada et al. (2006) [17] and Bhattacharjee et al. (2011) [18] also investigated the use of micropiles to increase the bearing capacity of footing. An experiment and computer study were conducted by Esmaeili et al. (2013) [4] on micropile-reinforced embankments. They found the best micropile configuration and the factor of safety for the embankment.

In addition, Rose et al. (2010) [19] developed a new method to calculate the axial group capacity of a group of micropiles placed around the edge of a clayey soil mass with a higher slenderness ratio. Han and Shu (2006) [20] investigated the compression and tension behavior of micropiles. Abd Elaziz and EI Naggar (2014) [12] used full-scale field testing and numerical analysis to examine the group behavior of hollow bar micropiles on stiff clay deposits.

Micropile Type D simulation is different from micropile Type A in that micropile Type D denotes a two-step grouting process. After the first grout is deposited and allowed to harden, an additional grout is injected using a Manchette tube at a pressure ranging from 2 to 8 MPa. When pressure grout is applied to cohesionless soil, some of the loosened soil is replaced and permeated, which results in the production of a cement paste that resembles cake along the grout–soil interface, improving the bond. The soil surrounding the borehole appears to be re-compacted or re-densified as a result of pressure grouting [21,22]. The diameter of the effective micropile following post-grouting is determined by the type of soil and the amount of grouting pressure applied; radial expansion causes the drilled hole diameter to stretch from (D) to (αc D).

Jang and Han (2014, 2015) [23,24] introduced the concept of a waveform micropile (Type D), which integrates the jet grouting technique with a conventional micropile (Type A), as depicted in Figure 1. This method creates wave-shaped grout sections, referred to as shear keys, by enlarging specific areas of the grout. These shear keys enhance shaft resistance at the interface between the ground and the grout.

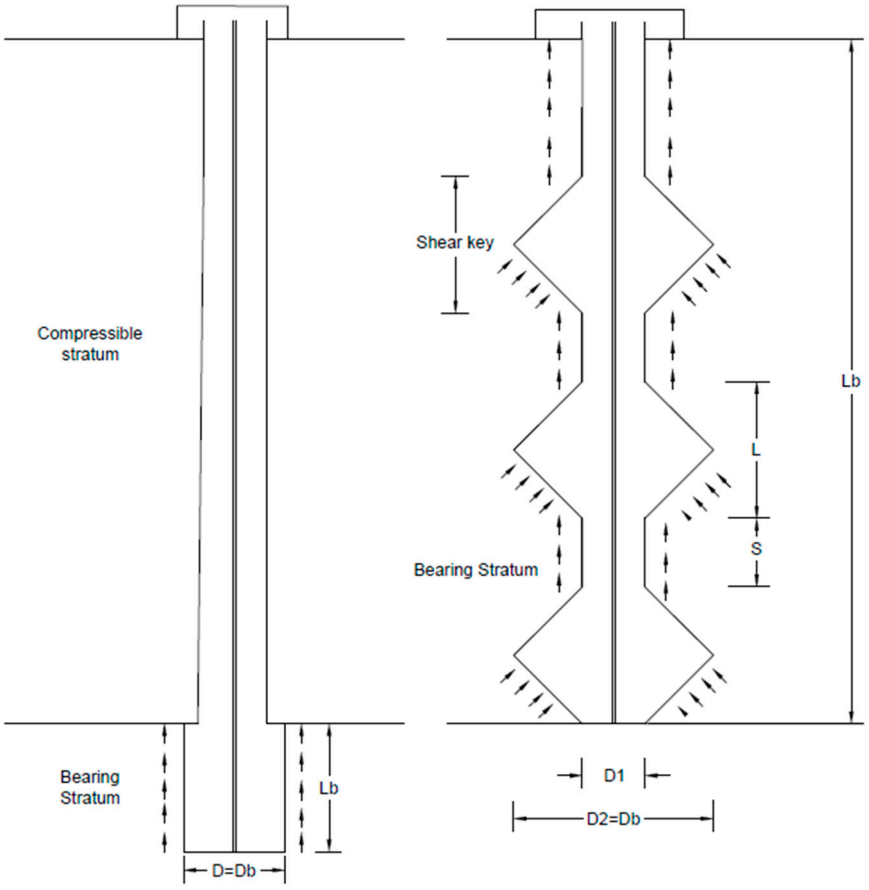


**Figure 1.** Conventional micropile (CM) and waveform micropile (WM) schematics [8].

This study aims to gain insight into the axial-load-carrying capacity and load-transfer mechanism of vertical and inclined group micropiles (Type D) under vertical loads. For this purpose, the finite-element (FE) analyses were performed to examine the behavior of the micropiles in layered soils. The spacing between micropiles, micropile inclination, and micropile diameters were considered in the analyses. The practical implications of the findings and the design considerations are discussed in detail. The results provide keys to understanding the load transfer mechanism of the inclined group micropiles and the displacement with depth.

## 2. Materials and Methods

### *2.1. Case Study Description*

Generally, to ensure the program's output accurately represents the studied reference case, it must undergo validation and verification through a series of studies before addressing geotechnical engineering problems or conducting parametric analyses using the finite element method (FEM). These reference cases may include laboratory tests on scaled models of the prototype structure or the results of field prototype tests. The present section focuses on the verification process of Midas Gts-Nx software with a reference study case representing field test conditions of a waveform micropile subjected to axial loading implemented by Jang and Han (2018) [8]. The waveform micropile has been embedded in layered soils. The soil stratification started with fill material (a mixture of soft to medium dense and well silty gravel) with a depth of about 4.5 m, followed by about 3 m thick of gravelly sand (deposit soil). Then, the weathered soil layer was 0.5 m thick and consisted of fine and coarse sand, while the last layer was weathered rock. The depth of the groundwater table was equal to about 4.7 m below the ground surface. On the other hand, the waveform

micropile length was 8 m, the diameter of shear key was 500 mm (outer diameter, D1), and the pile shaft was 300 mm (inner diameter, D2). Additionally, the length of shear key and the spacing between shear keys were the same and equal to 2D1.

### 2.2. Constitutive Models and Material Parameters

The elastic linear perfectly plastic Mohr–Coulomb (MC) constitutive model is among the most commonly used approaches in geotechnical engineering. It requires only a few parameters to characterize the behavior of soils and rocks [25–28]. This model assumes constant stiffness for each soil layer, making it a practical and efficient choice for a wide range of applications, as it allows for relatively quick computations. The MC model employs a non-associated flow rule, ignoring the effects of intermediate stresses beyond the principal ones. Elasticity is defined by two parameters: Young's modulus and Poisson's ratio, while the failure criteria are governed by cohesion and the friction angle. Additionally, the dilatancy angle is introduced as a parameter to account for irreversible volume changes and plastic deformation of the ground, reflecting the non-associated flow rule [29,30]. However, the Mohr–Coulomb model is used for simulating the soil. The soil properties are adopted by using the standard penetration test and are presented in Table 1. On the other hand, linear elastic models are adopted for simulating the micropile. The structural micropile parameters used in the numerical modelling are presented in Table 2.

**Table 1.** Soil properties for the field test (Adapted from Jang and Han (2018) [8]).

| Soil Layers Properties | Fill | Deposit | Weathered Soil | Weathered Rock |
|---|---|---|---|---|
| Depth: m | 0–4.5 | 4.5–7.5 | 7.5–8.0 | 8.0–15.0 |
| Unit weight ($\gamma$) (kN/m$^3$) | 18 | 19 | 20 | 21 |
| Elastic modulus (kN/m$^2$) | 22,800 | 34,800 | 51,600 | 450,000 |
| Poisson's ratio ($\nu$) | 0.3 | 0.3 | 0.3 | 0.28 |
| Cohesion (c) | 0.02 | 0.02 | 10 | 50 |
| Angle of internal friction ($\varphi$) | 30 | 35 | 33 | 39 |

**Table 2.** Micropile parameters used in analysis.

| Parameters | Value | Unit |
|---|---|---|
| Total unit weight, $\gamma$ | 24 | kN/m$^3$ |
| Modulus of elasticity, E | $30 \times 10^6$ | kN/m$^2$ |
| Poison's ratio, $\nu$ | 0.2 | - |

### 2.3. Finite Element Analysis

Numerical analyses were conducted to represent the micropile and soil layers using the Midas Gts-Nx finite element software. The mesh size was determined to be 10 m in both transverse and longitudinal directions, whereas the vertical dimension was 15 m. The dimensions were selected to make sure that they were sufficiently large to minimize boundary effects in the analysis results. The determination of these dimensions involved a sensitivity analysis [31,32]. Additionally, the soil model treated all directions of movement as free to move at the ground surface while remaining motionless at the bottom boundary. In contrast, the vertical boundaries were immobile in the direction perpendicular to them. It is worth mentioning that the fine mesh was used around the micropile base and the micropile circumference to achieve the best solution and capture the system's performance. As a result, the mesh had 20,294 elements and 3966 nodes. Figure 2 displays the 3D numerical model. Notably, the load was applied as prescribed displacement in the numerical modelling with a value of 35 mm, which corresponded to the final displacement estimated from the field test. Furthermore, the numerical model for the micropile included elements

of waveform grout, inner steel rebar, and the interface between the pile and soils. The strength reduction factor of the interface element ($R_{int}$) was comparable to that of cohesive and granular soils, or less. Therefore, the $R_{int}$ was taken to be equal to 0.67 in this study [33].

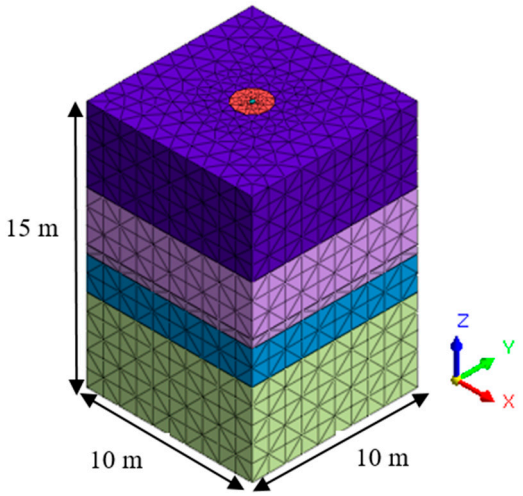


**Figure 2.** The 3D finite element model.

### *2.4. Construction Stages*

The numerical modeling process was carried out in three stages. First, geostatic stresses were initialized to replicate in situ stress conditions, with displacements reset to zero to focus solely on micropile behavior. During this stage, the rigid interface was activated, and the plane interface was deactivated to ensure smooth model operation. The second stage entailed modifying the micropile's characteristics and assigning its specific properties. In the final stage, a prescribed displacement load was applied incrementally until failure occurred, with the plane interface activated for this stage.

### *2.5. Verification of the Numerical Model*

The comparison of load–settlement curves from the numerical model and the experimental work is shown in Figure 3. The two curves exhibited a satisfactory degree of agreement. This alignment is important because it shows a good level of accuracy, showing that Midas GTs-Nx software can model complicated geotechnical problems well.

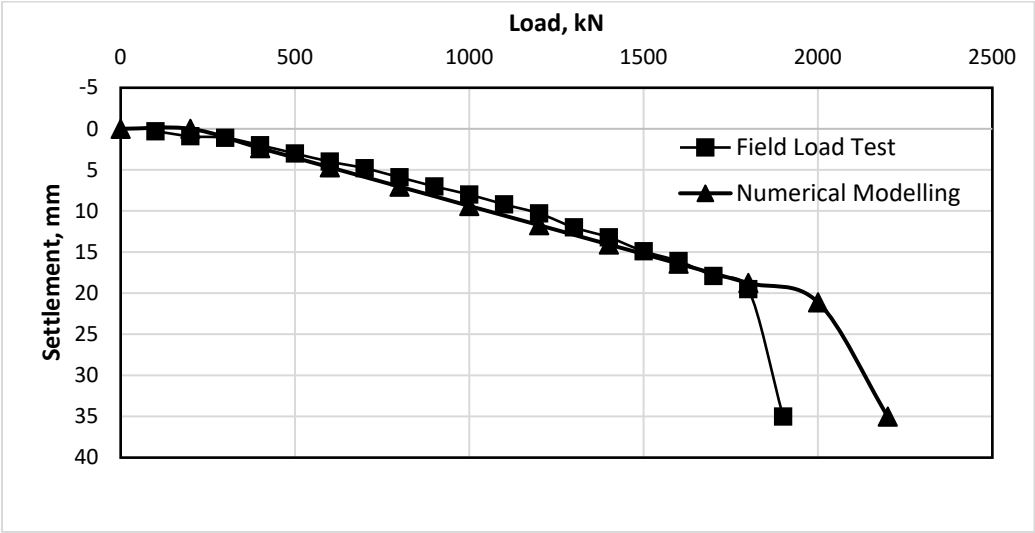


**Figure 3.** Load settlement curves from the numerical and field load tests.

## 3. Parametric Studies

A series of parametric studies were investigated to understand the behavior of micropile group (Type D) in layered soils with varying spacing ratio (S/D), inner diameter (Di), and the inclination angles (α). Table 3 presents all the parametric studies of this research. In 3D finite element analysis, the same soil layer properties and micropile characteristics, as well as constitutive models, as described for the validation model, were used. In addition, the same construction stages were established as mentioned in Section 2.3. Additionally, the micropile length (L) was 10 m, the distance from the micropile top (h1) to the first shear key was 1 m, the spacing between shear keys (h2) was 1 m, and the outer diameter (Do) was 0.45 m. Moreover, the micropile cap dimensions (L = B) were 3 m× 3 m and 0.3 m thickness (t). Figure 4 shows the vertical and inclined micropiles schematics.

**Table 3.** Parameters used in the parametric study.

| Analysis Series for a Research Plan | Range of Varying Parameters |
|---|---|
| Micropile spacing ratio S/D | 3, 5, and 7 |
| Inner diameter ($D_i$) | 0.1, 0.2, and 0.3 |
| Micropile inclination angles (α) | 0°, 10°, 20°, and 40° |

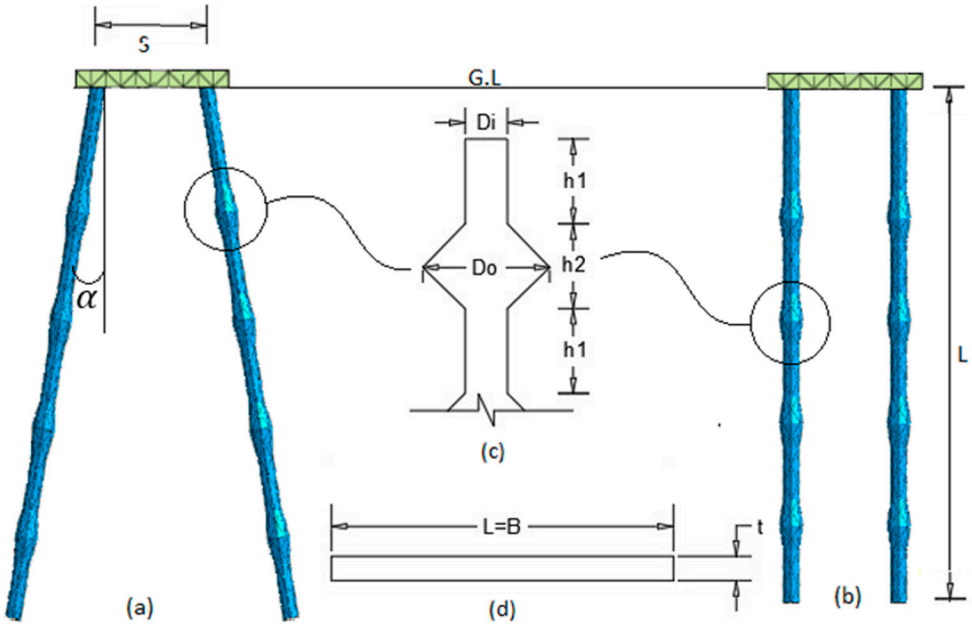


**Figure 4.** The 3D plan of the micropile group (Type D): (**a**) inclination, (**b**) vertical, (**c**) micropile details, and (**d**) micropile cap schematic.

## 4. Results and Discussion

### *4.1. Axial Displacement of Micropiles*

Many different parameters were studied to understand the behavior of the axial settlement of the vertical and inclined micropile groups. Figure 5a–d illustrate the axial settlements along the micropile depth for different micropile diameters, 0.3, 0.2, and 0.1 m, with different micropile angles, 0°, 10°, 20°, and 45°. The relationships show that a micropile's diameter significantly influences axial settlement due to its effect on the load transfer mechanism, stiffness, and interaction with the surrounding soil. As a result of a larger diameter, micropile Type D has a greater cross-sectional area and structural stiffness, which reduces elastic compression under load. Additionally, a larger diameter reduces the stress concentration in the soil surrounding the pile, minimizing soil deformation and settlement.

For vertical micropiles and micropiles with 10° and 20° inclination angles, the micropiles stiffness increased when the micropiles diameter increased. However, the axial displacement was approximately constant as the micropile diameter increased for an inclination angle equal to 45° for a different S/D ratio.

Furthermore, the effect of the vertical and inclined micropile spacing (S/D) had a significant effect when the micropiles diameters were 0.1 m and 0.2 m. It can be concluded that for closer spacings, micropile stress zones overlapped, resulting in the increased soil stress and reduced load-carrying efficiency of each pile. The overlapping stress zones can lead to greater soil deformation and higher overall axial settlement for the group. The load distribution among micropiles became less effective, reducing the efficiency of the pile group. However, when micropiles were spaced farther apart, their stress zones remained independent, minimizing interference between individual piles. Additionally, for 0.3 m diameter, there was no significant increase or reduction of the axial settlement for vertical and inclined micropiles for different micropile spacings.

Figure 6 illustrates the distribution of axial settlement along vertical and inclined micropiles from Midas Gts-Nx in the case of 0.3 m diameter, 20° inclination angle, and S/D = 5.

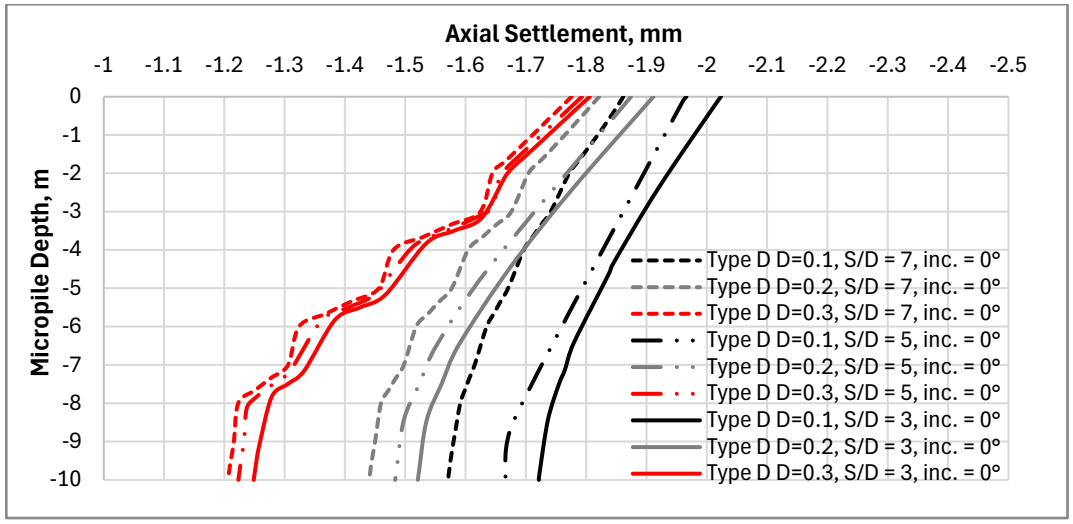


(**a**)

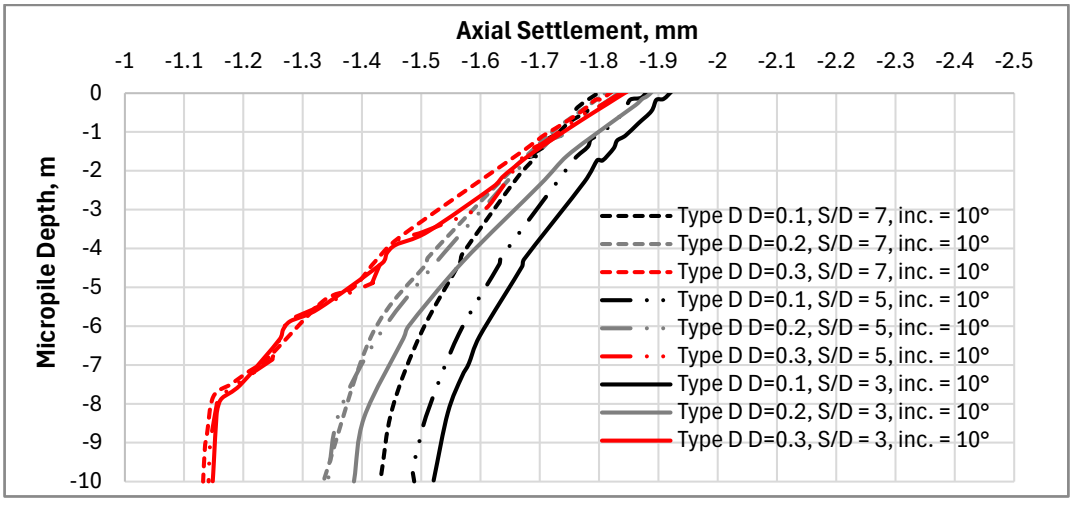


(**b**)

**Figure 5.** *Cont.*

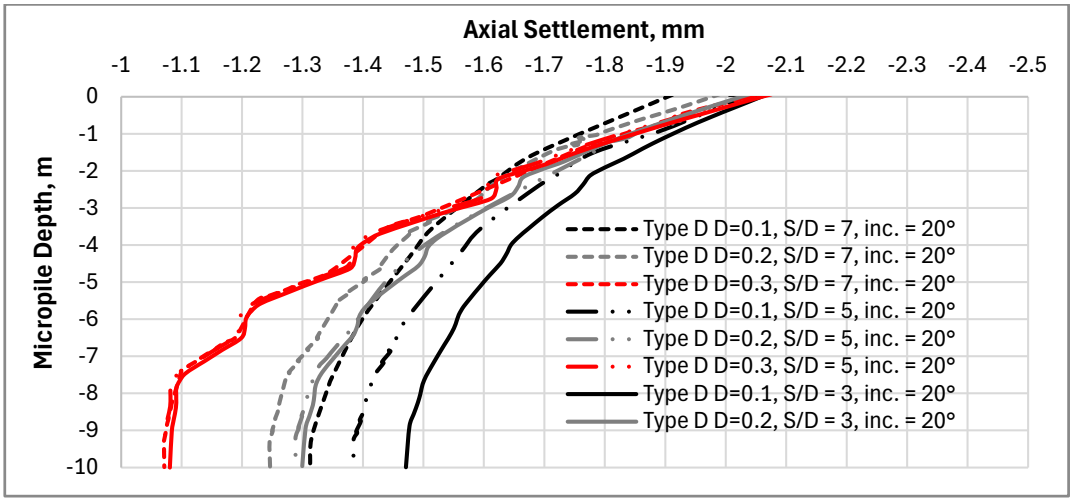


(**c**)

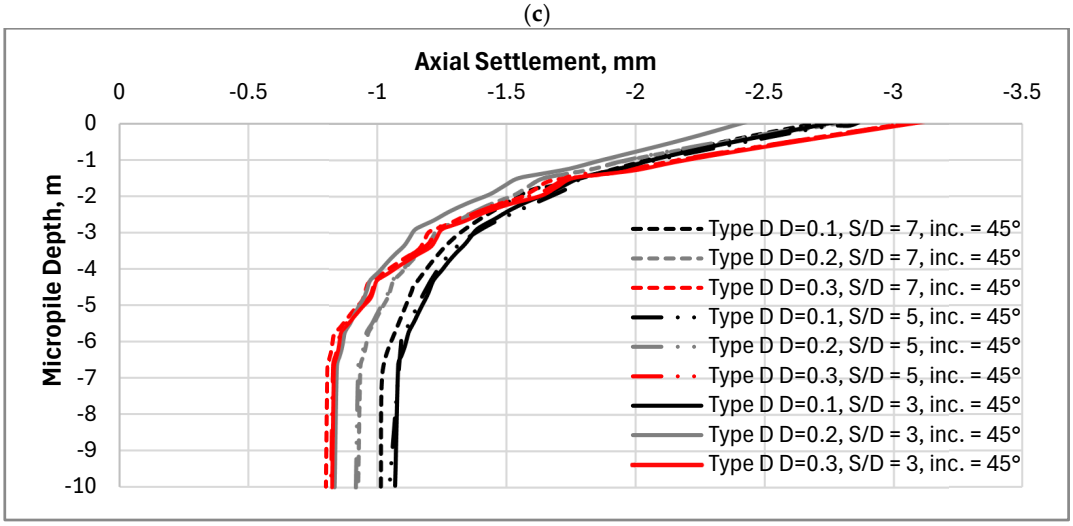


(**d**)

**Figure 5.** The relationship between the axial displacement and micropile depth with different micropile angles: (**a**) vertical micropile; (**b**) inclination angle 10°; (**c**) inclination angle 20°; and (**d**) inclination angle 45°.

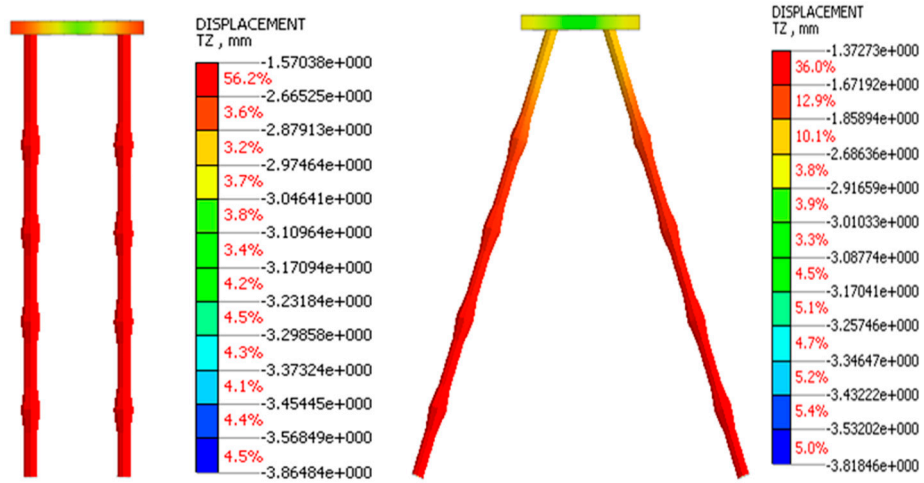


(**a**) (**b**)

**Figure 6.** Axial settlement distribution for (**a**) vertical and (**b**) inclined micropiles with 0.3 m diameter, 20° inclination angle, and S/D = 5.

### *4.2. Axial Force of Micropiles*

Figure 7a–d illustrate the impact of micropile diameter (D), spacing-to-diameter ratio (S/D), and inclination angle (inc) on axial force distribution along the depth of micropiles.

Larger diameters (D = 0.3) showed up to 200% higher initial axial forces compared to smaller diameters (D = 0.1) and retained about 40–50% of their load at 10 m depth, whereas smaller piles retained only 10–15%, reflecting rapid dissipation.

Closely spacing (lower S/D) reduced group effects, leading to lower axial force per micropile, whereas increased spaced micropiles (higher S/D) enhanced load-sharing interactions in the case of vertical subjected to vertical loads only. Wider spacing (S/D = 7) enhanced group effects, increasing axial forces by 10–15% at the surface compared to closer spacing (S/D = 3). However, the wider spacing caused reductions in axial force for inclined micropiles under vertical loads only. Increasing the spacing between micropiles enables them to act more independently, which in turn decreases the axial force exerted on each micropile under vertical loading.

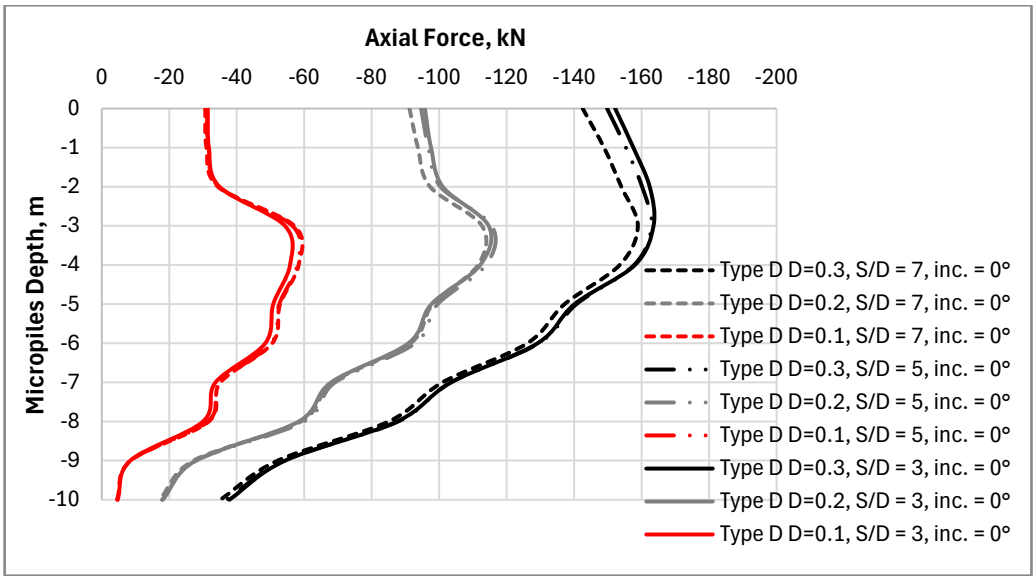


(**a**)

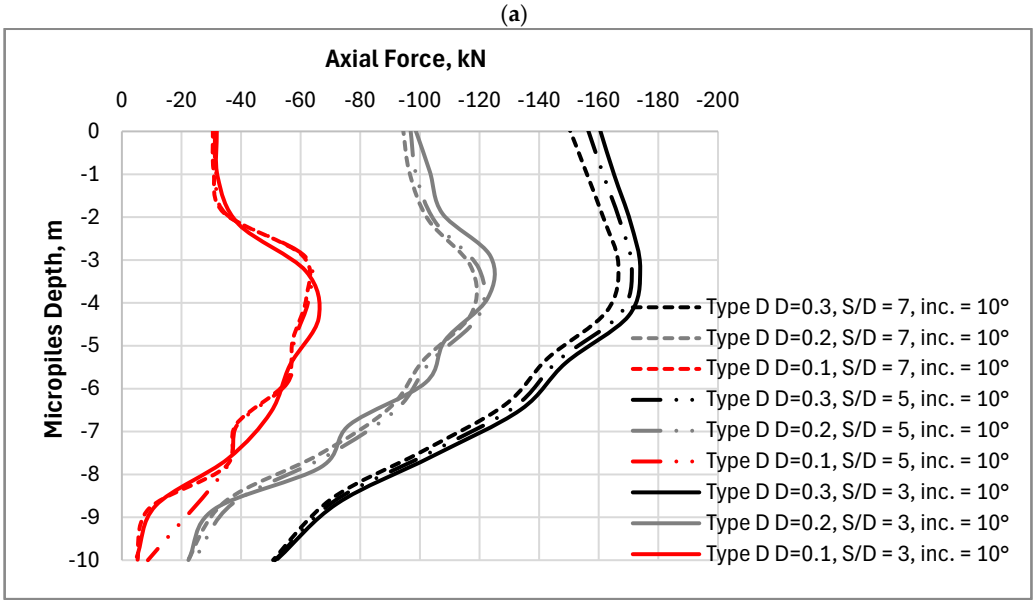


(**b**)

**Figure 7.** *Cont.*

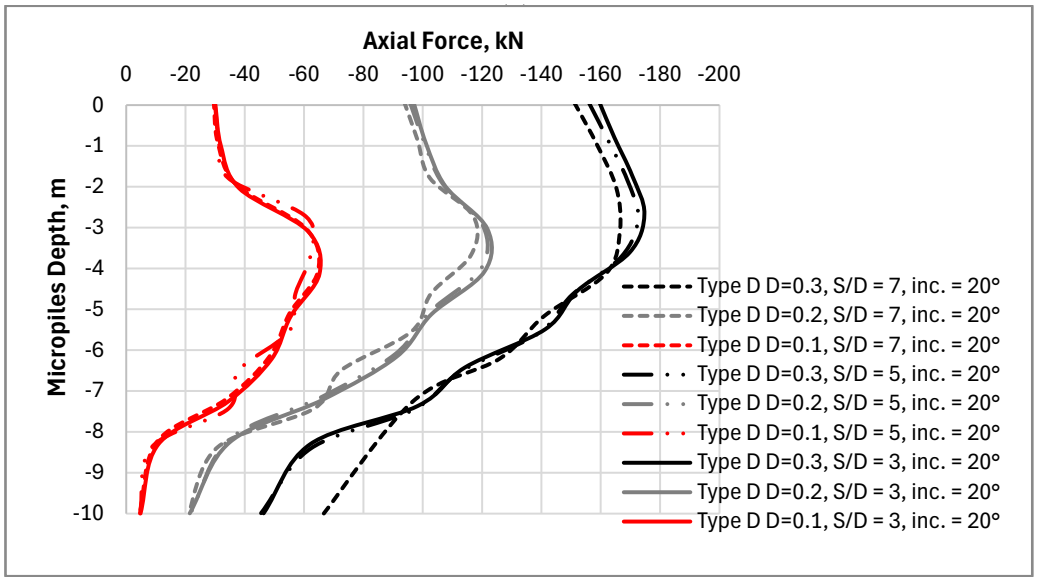


(**c**)

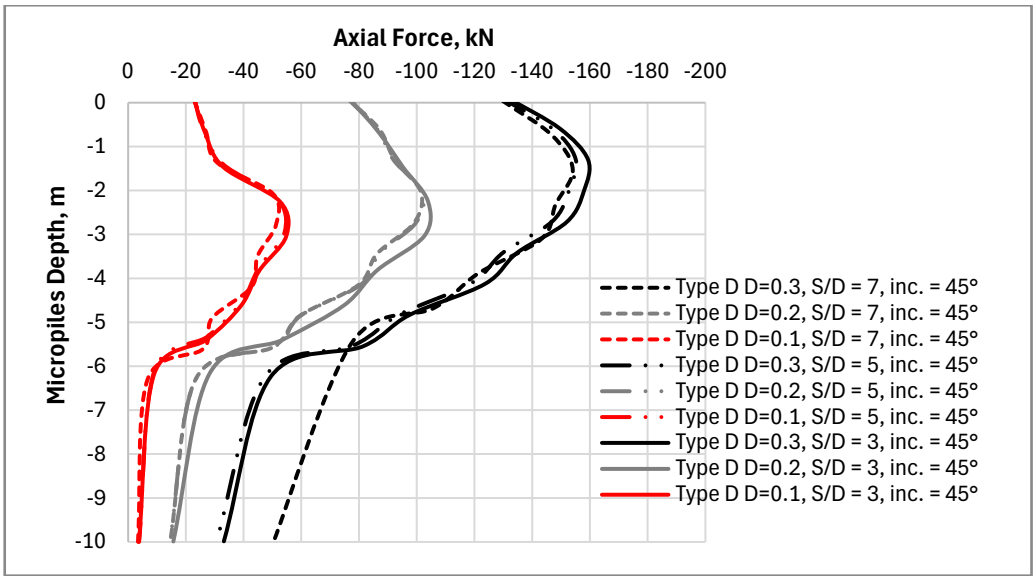


(**d**)

**Figure 7.** The relationship between the axial force and micropile depth with different micropile angles: (**a**) vertical micropile; (**b**) inclination angle 10°; (**c**) inclination angle 20°; and (**d**) inclination angle 45°.

Inclination amplified force dissipation, with inclined piles (inc = 45°) losing up to 70–80% of their load by 10 m depth, compared to only 40–50% for vertical piles (inc = 0°). As the inclination angle increased from vertical (0°) to 45°, axial forces dissipated more rapidly due to increased lateral load transfer to the surrounding soil, reducing the vertical load-bearing capacity.

These results highlight the importance of optimizing micropile configuration based on load requirements, where vertical piles are ideal for compressive loads, and inclined piles are better suited for lateral stability and load dispersion.

Figure 8 illustrates the distribution of axial force along vertical and inclined micropiles from Midas Gts-Nx in the case of 0.3 m diameter, 20° inclination angle, and S/D = 5.

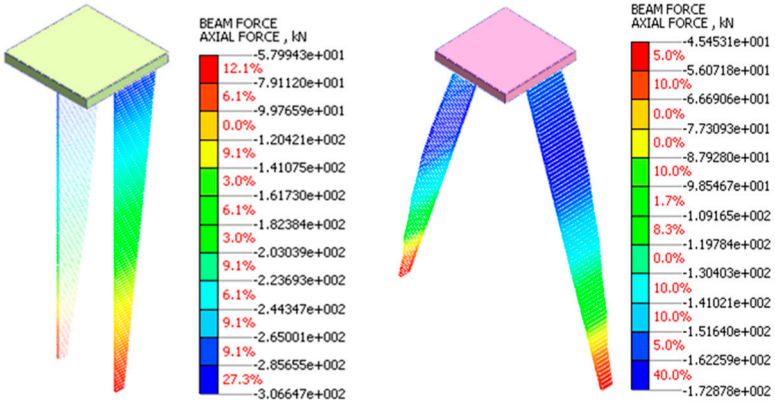


(**a**) (**b**)

**Figure 8.** Axial force distribution for (**a**) vertical and (**b**) inclined micropiles with 0.3 m diameter, 20° inclination angle, and S/D = 5.

### *4.3. Lateral Displacement of Micropiles*

Figure 9a–d show the lateral displacement of the micropile behavior at different inclination angles. It can be noted that the inclined micropiles (batter piles) exhibited greater lateral displacement compared to vertical ones due to their orientation.

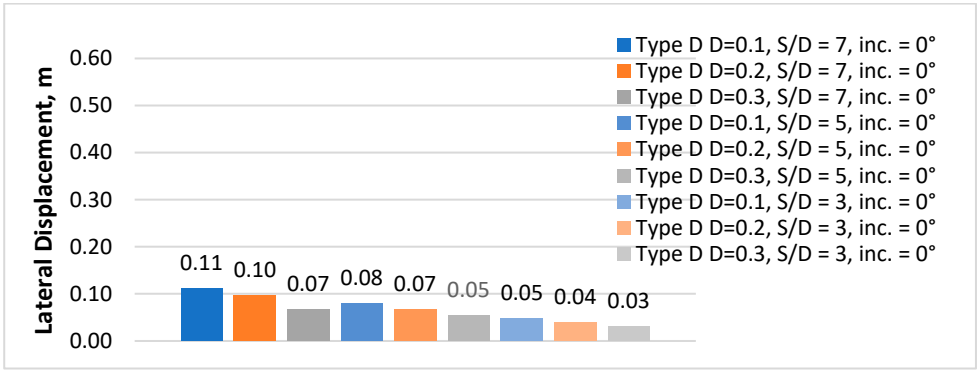


(**a**)

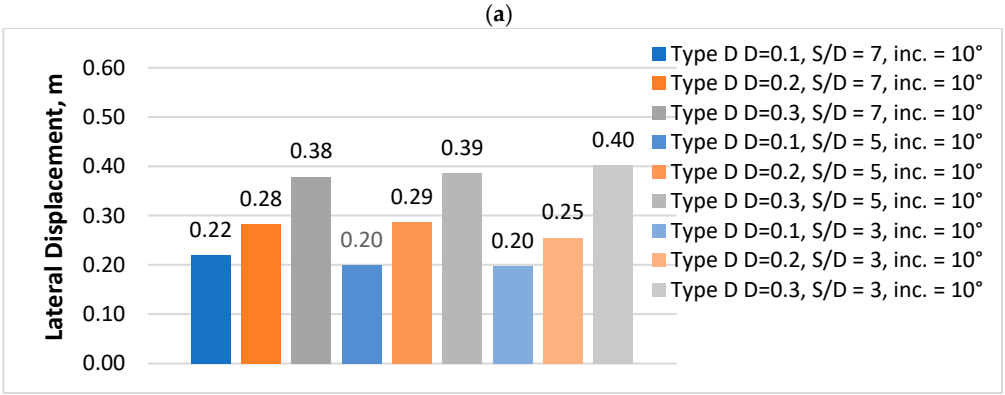


(**b**)

**Figure 9.** *Cont.*

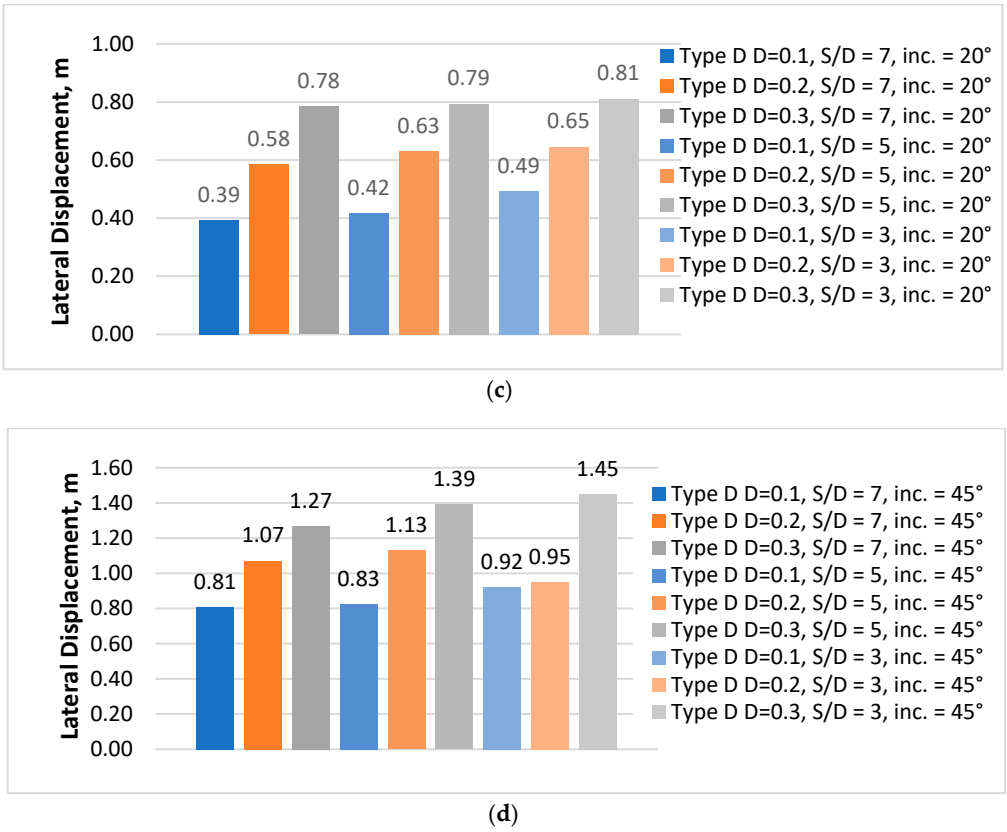


**Figure 9.** The relationship between the lateral displacement and micropile depth with different micropile angles: (**a**) vertical micropile; (**b**) inclination angle 10°; (**c**) inclination angle 20°; and (**d**) inclination angle 45°.

Larger diameters provided increased stiffness, reducing lateral displacements under equivalent loads when the inclination angles increased from 0 to 20. The larger surface area enhanced frictional and passive soil resistance, further mitigating displacement. For 45 inclination angles, the amount of deflection increased with the angle of inclination, as the lateral component of the axial load increased with the inclination. This was a result of micropile groups, where interaction effects can amplify or mitigate lateral displacements depending on pile spacing, inclination, and loading conditions. When the micropile was inclined, axial loading not only induced axial stress but also generated lateral forces (due to the component of the axial load perpendicular to the micropile axis). This lateral force caused the micropile to deflect sideways.

The lateral deflection at the micropile head (or the connection point with the pile cap) was greatest and decreased along the shaft. Additionally, there was no visible effect of micropile spacing for all inclined micropiles that had the same diameter and inclination angle. However, the deflection increased with the increase in micropile inclination due to the vertical loads. For vertical micropiles, the lateral displacements reduced to about 37.5% and 54.5% when the micropile spacing reduced from 7 to 5 and 3 m, respectively, for 0.3 m diameter, 30% and 40% for 0.2 m diameter, and 28.5% and 42.8% for 0.1 m diameter (Figure 9a). In addition, Figure 10 illustrates the distribution of lateral displacement along vertical and inclined micropiles from Midas Gts-Nx in the case of 0.3 m diameter, 20° inclination angle, and S/D = 5.

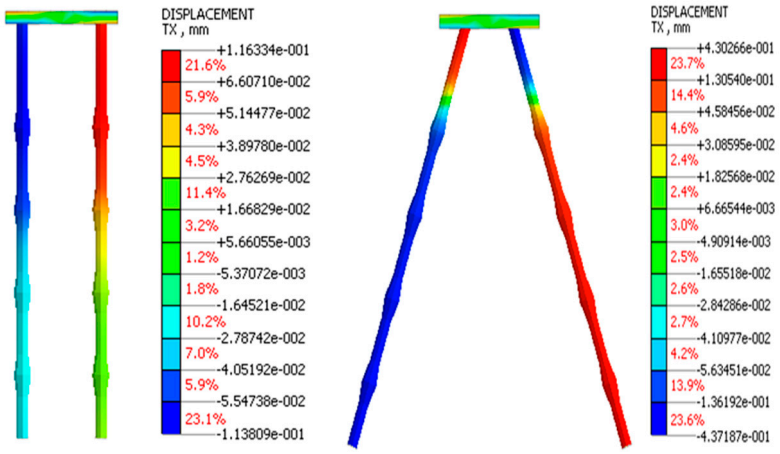


(**a**) (**b**)

**Figure 10.** Lateral displacement distribution for (**a**) vertical and (**b**) inclined micropiles with 0.3 m diameter, 20° inclination angle, and S/D = 5.

### *4.4. Bending Moment of Micropiles*

Figure 11a–d demonstrate the relations between bending moment and depth for vertical and inclination micropiles. These relations indicate that bending moment reduced as the micropile diameter increased for all micropile conditions.

Additionally, the bending moment increased with the increase in micropile inclination in the case of applying vertical loads. For D = 0.3 m; S/D = 7; and inclination angles of 10°, 20°, and 45°, the incremental ratio increased to be 61.5%, 72.1%, and 89.2%, respectively, more than vertical micropiles. As the inclination angle grew, a larger horizontal component of the applied load generated higher lateral forces, while the eccentricity caused by the pile's inclination amplified bending stresses.

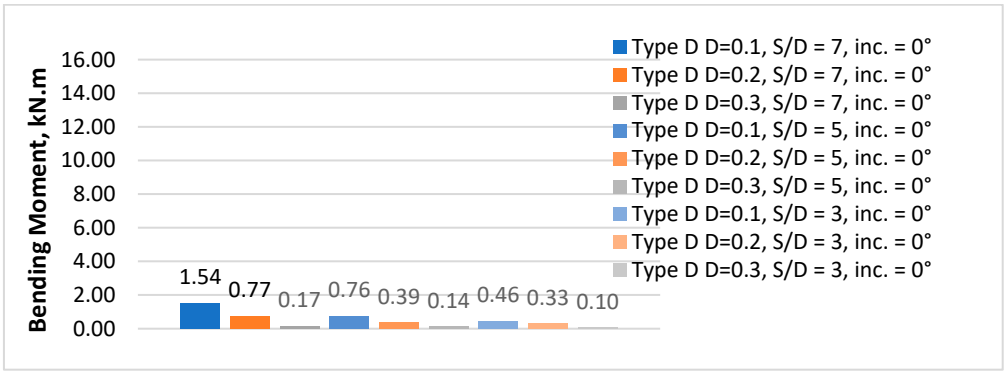


(**a**)

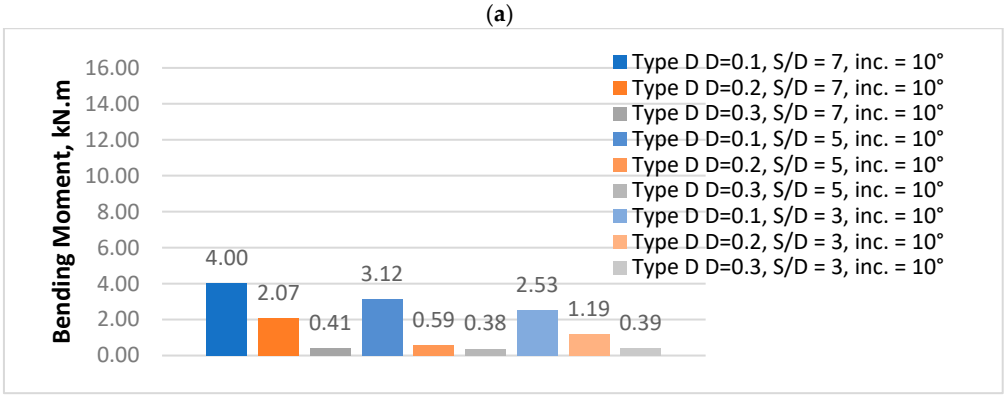


(**b**)

**Figure 11.** *Cont.*

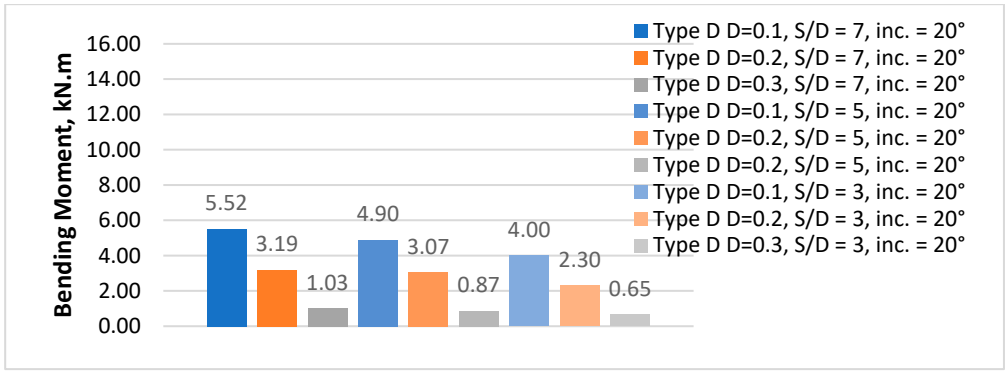


(**c**)

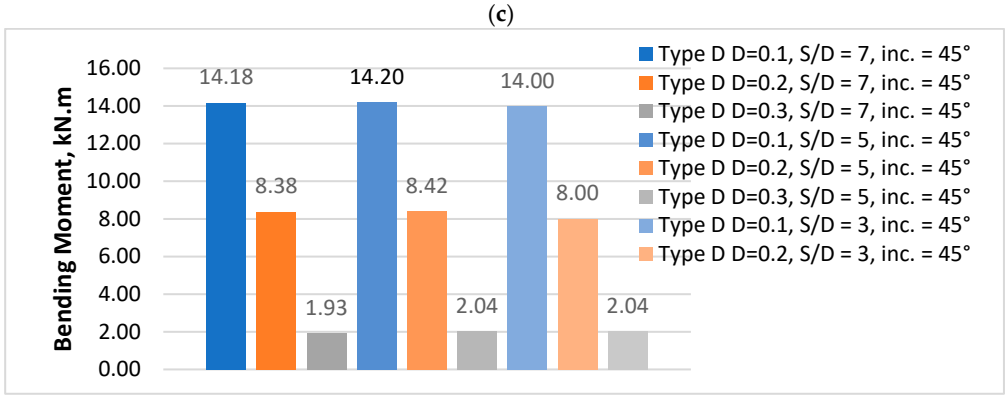


(**d**)

**Figure 11.** The relationship between the bending moment and micropile depth with different micropile angles: (**a**) vertical micropile; (**b**) inclination angle 10°; (**c**) inclination angle 20°; and (**d**) inclination angle 45°.

Furthermore, when the inclination angle of micropiles in a group exceeded 20 degrees, the spacing between micropiles in a group had minimal impact on the bending moment. This occurred because the load was redistributed more effectively into axial forces, reducing the lateral forces that typically induce bending.

Figure 12 illustrates the distribution of bending moment along vertical and inclined micropiles from Midas Gts-Nx in the case of 0.3 m diameter, 20° inclination angle, and S/D = 5.

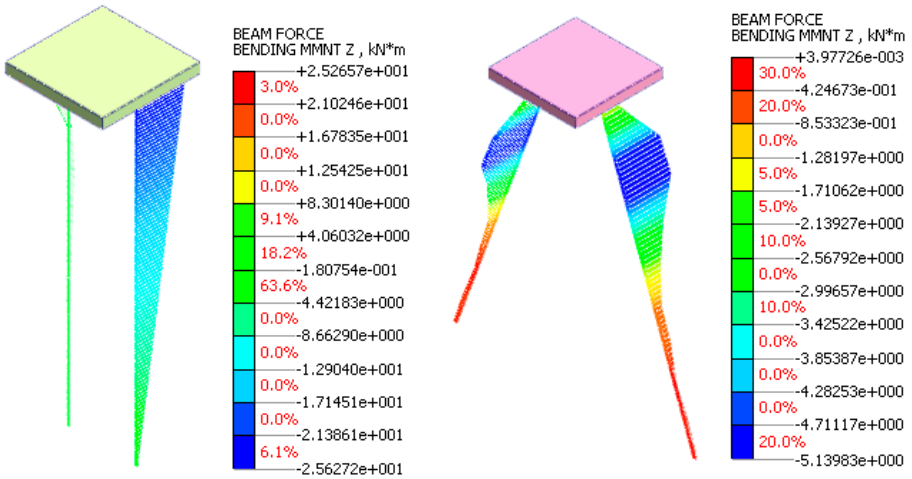


(**a**) (**b**)

**Figure 12.** Bending moment distribution for (**a**) vertical and (**b**) inclined micropiles with 0.3 m diameter, 20° inclination angle, and S/D = 5.

## 5. Conclusions

A finite element analysis was established to understand the load transfer mechanism of micropiles (Type D) subjected to vertical loads under different parametric studies, among which are micropile inclination, the spacing between micropiles, and micropile diameters. This study draws the following conclusions based on its results:

1. A micropile's performance is greatly improved by increasing its diameter since it improves load transfer, increases structural stiffness, and lessens soil deformation and settlement.
2. The stiffness of micropiles that were vertical and those with inclination angles of 10° and 20° increased as the diameter of the micropile grew. Nevertheless, the axial displacement was almost constant for a 45° inclination angle, independent on the micropile diameter.
3. For diameters of 0.1 m and 0.2 m, micropile spacing (S/D) had a substantial impact on axial settlement and load efficiency; broader spacing improved soil utilization, while closer spacing resulted in stress overlap. Axial settlement was not significantly affected by spacing for the 0.3 m diameter.
4. Compared to lower diameters (D = 0.1), larger micropile diameters (D = 0.3) showed much stronger initial axial forces and superior load retention at depth, holding 40–50% of their load at 10 m.
5. Lower axial forces per micropile were the consequence of minimizing group effects by a reduction in the space between micropiles (lower S/D ratio). On the other hand, under vertical stresses, load-sharing interactions were enhanced by increasing the spacing (greater S/D ratio). In comparison to closer spacing (S/D = 3), group effects were more noticeable at a wider separation (S/D = 7), increasing axial forces at the surface by 10–15%.
6. By improving frictional and passive soil resistance, larger micropile sizes increased stiffness and decreased lateral displacements for inclination angles up to 20°. Furthermore, because of the increased lateral component of axial stresses at a 45° inclination angle, lateral deflection increased. Group interaction effects were influenced by loading circumstances, pile spacing, and inclination.
7. Bending stresses were amplified by increasing eccentricity and horizontal loads, and the bending moment increased as the micropile inclination angle increased. Furthermore, because load dispersal lowered lateral forces and bending, micropile spacing had no effect on the bending moment for inclination angles larger than 20°.

**Funding:** This research received no external funding.

**Institutional Review Board Statement:** Not applicable.

**Informed Consent Statement:** Not applicable.

**Data Availability Statement:** The data presented in this study are available on request from the corresponding author. The data are not publicly available due to privacy.

**Conflicts of Interest:** The author declares no conflict of interest.

## References

1. Bruce, D.A.; DiMillio, A.F.; Juran, I. *Introduction to Micropiles: An International Perspective*; ASCE: Reston, VA, USA, 1995.
2. FHWA. *Micropile Design and Construction*; Publ. No. FHWA NHI-05-039; National Highway Institute: Washington, DC, USA, 2005.
3. Tsukada, Y.; Miura, K.; Tsubokawa, Y.; Otani, Y.; You, G.L. Mechanism of Bearing Capacity of Spread Footings Reinforced with Micropiles. *Soils Found.* **2006**, *46*, 367–376. [CrossRef]
4. Esmaeili, M.; Nik, M.G.; Khayyer, F. Experimental and Numerical Study of Micropiles to Reinforce High Railway Embankments. *Int. J. Geomech.* **2013**, *13*, 729–744. [CrossRef]

5. Wu, W.; Di, T.; Yang, X.; El Naggar, M.H.; Zhang, Y. Revised pile-pile mutual interaction factors for seismic analysis of end-bearing pile groups embedded in saturated stratum. *Soil Dyn. Earthq. Eng.* **2024**, *182*, 108745. [CrossRef]
6. Zhang, Y.; Ji, H.; Zhang, L.; El Naggar, M.H.; Wu, W. Identification of bored pile defects utilizing torsional low strain integrity test: Theoretical basis and numerical analysis. *J. Rock Mech. Geotech. Eng.* 2024, *in press*. [CrossRef]
7. Liu, X.; Tang, L.; Wu, W.; El Naggar, M.H.; Zhang, Z.; Wang, H.; Sun, J. Theoretical Investigation of Dynamic Pile–Soil Interaction in Torsion Considering Continuity of Heterogeneous Soil. *Int. J. Numer. Anal. Methods Geomech.* 2024; *in press*. [CrossRef]
8. Jang, Y.E.; Han, J.T. Field Study on Axial Bearing Capacity and Load Transfer Characteristic of Waveform Micropile. *Can. Geotech. J.* **2018**, *55*, 653–665. [CrossRef]
9. Juran, I.; Bruce, D.A.; Dimillio, A.; Benslimane, A. Micropiles: The state of practice. Part II: Design of single micropiles and groups and networks of micropiles. *Ground Improv.* **1999**, *3*, 89–110. [CrossRef]
10. Armour, T.; Groneck, P.; Keeley, J.; Sharma, S. *Micropile Design and Construction Guidelines—Implementation Manual*; Report No. FHWA-SA-97-070; Federal HighwayAdministration–US Department Transportation: Vancouver, WA, USA, 2000; p. 376.
11. Rose, A.; Taylor, R.; El Naggar, M. Numerical modelling of perimeter pile groups in clay. *Can. Geotech. J.* **2013**, *50*, 250–258. [CrossRef]
12. Abd Elaziz, A.Y.; El Naggar, M.H. Geotechnical capacity of hollow-bar micropiles in cohesive soils. *Can. Geotech. J.* **2014**, *51*, 1123–1138. [CrossRef]
13. Alnuaim, A.M.; El Naggar, H.; El Naggar, M.H. Performance of micropiled raft in sand subjected to vertical concentrated load: Centrifuge modeling. *Can. Geotech. J.* **2014**, *52*, 33–45. [CrossRef]
14. Kyung, D.; Lee, J. Interpretative Analysis of Lateral Load-Carrying Behavior and Design Model for Inclined Single and Group Micropiles. *J. Geotech. Geoenviron. Eng.* **2018**, *144*, 04017105. [CrossRef]
15. Li, Z.; Kotronis, P.; Escoffier, S.; Tamagnini, C. A hypoplastic macroelement formulation for single batter piles in sand. *Int. J. Numer. Anal. Methods Geomech.* **2018**, *42*, 1346–1365. [CrossRef]
16. Abbas, Q.; Kim, G.; Kim, I.; Kyung, D.; Lee, J. Lateral Load Behavior of Inclined Micropiles Installed in Soil and Rock Layers. *Int. J. Geomech.* **2021**, *21*, 1–13. [CrossRef]
17. Tsukada, Y.; Miura, K.; Tsubokawa, Y.; Ishito, M.; Nishimura, N.; Ohtani, Y.; You, G.L. Experimental investigation on the improvement of bearing capacity of surface footing with micropiles. In Proceedings of the 2nd International Workshop on Micropiles, Ube City, Japan, September 1999; pp. 139–148. Available online: https://www.ismicropiles.org/1999.asp (accessed on 31 December 2024).
18. Bhattacharjee, A.; Mittal, S.; Krishna, A.M. Bearing capacity improvement of square footing by micropiles. *Int. J. Geotech. Eng.* **2011**, *5*, 113–118. [CrossRef]
19. Rose, A.V.; Taylor, R.N. Modelling the axial capacity of micropiles at close spacing. In Proceedings of the 10th International Workshop of Micropile, Washington, DC, USA, 22–25 September 2010.
20. Han, J.; Ye, S.L. A field study on the behavior of a foundation underpinned by micropiles. *Can. Geotech. J.* **2006**, *43*, 30–42. [CrossRef]
21. Shong, L.S.; Chung, F.C. Design & construction of micropiles. In Proceedings of the Geotechnical Course for Pile Foundation Design & Construction, Ipoh, Malaysia, 29–30 September 2003; pp. 1–49.
22. Ayasrah, M.M.; Al-Karawi, A.; Qiu, H. Behavior of micropiles in layered soils. *AIP Conf. Proc.* **2024**, *3229*, 060003.
23. Jang, Y.E.; Han, J.T. Development on the Micropile for Applying to Artificial Ground above Railroad Site. *Adv. Sci. Technol. Lett.* **2014**, *55*, 43–46.
24. Jang, Y.E.; Han, J.T. Study of Load Capacity of Waveform Micropile by Centrifuge test. In Proceedings of the 25th International Offshore and Polar Engineering Conference, Kona, HI, USA, 21–26 June 2015.
25. Chen, W.F.; Saleeb, A.F. *Constitutive Equations for Engineering Materials. Volume 1: Elasticity and Modeling*; Elsevier: Amsterdam, The Netherlands, 1982.
26. Nguyen, V.Q.; Merifield, R.S. Undrained bearing capacity of surface footings near slopes. *Aust. Geomech.* **2011**, *46*, 77.
27. Lee, J.K.; Jeong, S.; Shang, J.Q. Undrained bearing capacity of ring foundations on two-layered clays. *Ocean Eng.* **2016**, *119*, 47–57. [CrossRef]
28. Qiu, H.; Qiu, R.; Luo, G.; Ayasrah, M.M.; Wang, Z. Study on the mechanical behavior of fluid–solid coupling in shallow buried tunnels under different biased terrain. *Symmetry* **2022**, *14*, 1339. [CrossRef]
29. Lade, P.V. Overview of constitutive models for soils. In *Soil Constitutive Models: Evaluation, Selection, and Calibration*; Yamamuro, J.A., Kaliakin, V.N., Eds.; ASCE Geotechnical Special Publication No. 128; ASCE: Reston, VA, USA, 2005; pp. 1–34.
30. Ti, K.; Huat, B.; Noorzaei, J.; Jaafar, M. A Review of Basic Soil Constitutive Models for Geotechnical Application. *Electron. J. Geotech. Eng.* **2009**, *14*, 1–18.
31. Qiu, H.; Wang, H.; Ayasrah, M.M.; Zhou, Z.; Li, B. Study on Horizontal Bearing Capacity of Pile Group Foundation Composed of Inclined and Straight Piles. *Buildings* **2023**, *13*, 690. [CrossRef]

32. Huang, W.; Liu, J.; Wang, H.; Ayasrah, M.; Qiu, H.; Wang, Z. Study on Dynamic Response of Inclined Pile Group Foundation under Earthquake Action. *Buildings* **2023**, *13*, 2416. [CrossRef]
33. Garbacz, A. Stress wave propagation throughout an interface: PCC composites-concrete substrate in repair system. *Archit. Civil. Eng. Environ.* **2010**, *3*, 35–44.